

# Continuous-wave Laser Thermography for Concrete Crack Evaluation under Moving Conditions

Keun-Young Jang<sup>1</sup>, Soonkyu Hwang<sup>2</sup>, Jiho Park<sup>2</sup> and Yun-Kyu An<sup>1,\*</sup>

<sup>1</sup>*Department of Architectural Engineering, Sejong University, Seoul, 05006, South Korea*

<sup>2</sup>*Department of Civil and Environmental Engineering, KAIST, Daejeon, 34141, South Korea*

[jj99137@sju.ac.kr](mailto:jj99137@sju.ac.kr); [soonkyu@kaist.ac.kr](mailto:soonkyu@kaist.ac.kr); [pjh742@kaist.ac.kr](mailto:pjh742@kaist.ac.kr); [yunkyu@sejong.ac.kr](mailto:yunkyu@sejong.ac.kr)

*\*Corresponding author*

## ABSTRACT

This paper presents a continuous-wave laser thermography (CLT) technique for concrete surface crack evaluation under moving conditions. The CLT technique is able to visualize and quantify surface cracks on moving concrete structures by generating a continuous-wave laser source and capturing infrared images at a fixed spatial point. Although the CLT system has spatially limited field of view, it can inspect the entire region of interest (ROI) of the moving target structure. To precisely quantify surface cracks, the data acquired from the entire ROI are integrated and subsequently processed by developing an instantaneous crack evaluation algorithm. In this study, concrete specimens with various macro- and micro-cracks are specially prepared and used to validate the proposed CLT technique. The test results reveal that various cracks are successfully visualized and quantified within 3% error ratio.

Keywords: Continuous-wave laser thermography, Concrete crack evaluation, Crack quantification, Moving target structure, Phase mapping, Non-destructive testing

## 1. INTRODUCTION

Concrete structures are inherently vulnerable to cracks. The surface cracks often gradually propagate along the depth direction of the concrete structure, allowing the water penetration. Such phenomena can pose severe debonding and corrosion damage, eventually reducing concrete strength. Thus, the surface crack width control is one of the main concerns in the structural health monitoring point of view.

Visual inspection by well-trained experts has been most widely used in the field, but it is quite labor-intensive, costly and cumbersome. Thus, a number of nondestructive inspection (NDI) methods have been proposed as alternatives. One of the widely accepted NDI methods is a vision image

method [1]. Although it is quite simple and cost-effective, the reliability of the results may be degraded depending on the image capture conditions such as capture angle, illuminance, undesired dust in the air or target surface and so on. Another promising NDI method is an ultrasonic method thanks to its high detectability to cracks [2]. However, the ultrasonic method typically requires the contact-type sensing mechanism especially for concrete in that the signal-to-noise ratio of the ultrasonic responses should be enhanced. Such contact sensing mechanism disturbs large area inspection and inaccessible area inspection. Moreover, inhomogeneity of concrete makes the responses difficult to be physically interpreted. An optical lamp-based infrared (IR) thermography has been also applied to concrete crack inspection [3]. However, its working distance is typically short due to the divergence characteristic of the optical heat source. Moreover, the high power heat source cannot be precisely controlled, making it difficult to inspect large inspection areas.

To overcome the aforementioned technical hurdles, continuous-wave laser thermography (CLT) technique is developed for concrete surface crack evaluation in this paper. The CLT technique has the following technical advantages over the existing NDI techniques: (1) Noncontact, noninvasive and remote inspection can be achieved; (2) Large target area can be effectively inspected by spatially scanning the CLT system itself; (3) Making-decision for crack evaluation can be instantaneously performed without accumulated baseline data; (4) Multiple cracks from macro- to micro cracks can be sensitively visualized by self-normalized phase mapping; and (5) Positive false alarm caused by environmental or surface disturbance can be minimized.

This paper is organized as follows. Chapter 2 introduces hardware of the CLT system and its working principle.

Chapter 3 explains an instantaneous crack evaluation algorithm. The effectiveness of the proposed CLT system is experimentally validated using a lab-scale concrete specimen with various macro- and micro-cracks described in Chapter 4. The paper concludes with a brief summary and discussions in Chapter 5.

## 2. CONTINUOUS-WAVE LASER THERMOGRAPHY SYSTEM

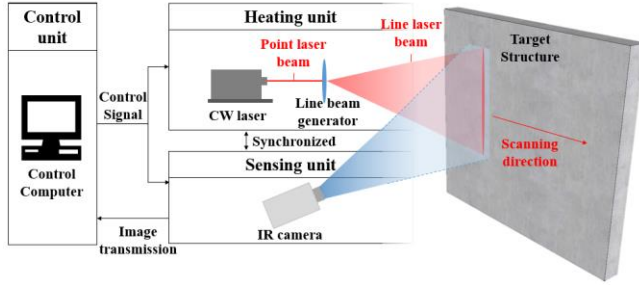


Figure 1. Schematics of the proposed continuous-wave laser thermography (CLT) system: CW denotes continuous-wave.

The CLT system is composed of excitation, sensing and control units, as shown in Figure 1. First, the continuous-wave laser emits a point laser beam, and the point laser beam is subsequently changed to a line shape beam through the line beam generator in the excitation unit once the control signal is transmitted from the control unit to the heating and sensing units. Then, the line laser beam is exerted onto a target concrete surface of interest, making it possible to generate thermal waves. The line laser beam can be precisely controlled and aimed onto the target area with little shape distortion even for a long target distance thanks to the directionality and non-divergence characteristics of the laser beam (An, 2013). Simultaneously, the IR camera in the sensing unit captures the corresponding thermal responses. Here, the entire region of interest (ROI) can be effectively inspected by spatially scanning the CLT system. Typically, thermal waves are quite locally generated on concrete materials with relatively small thermal conductivity (approximately 0.8W/m K), and the IR camera has limited field of view (FOV). Thus, the spatial scanning mechanism is necessary. If the CLT system can move along the target structure, even large ROI can be effectively covered. Note that the excitation and sensing units are all synchronized with the control unit as shown in Figure 1.

## 3. DEVELOPMENT OF AN INSTANTANEOUS CRACK EVALUATION ALGORITHM UNDER MOVING CONDITIONS

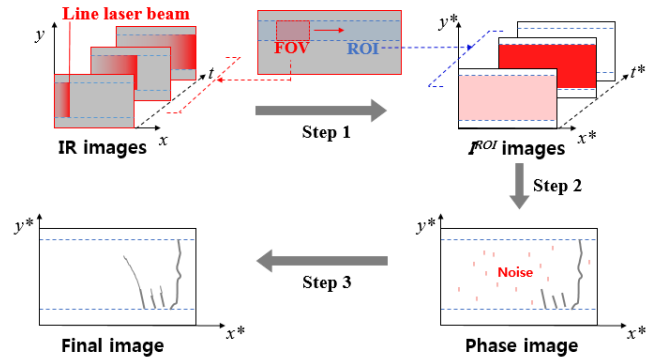


Figure 2. Overview of the instantaneous crack evaluation algorithm

This chapter describes the instantaneous crack evaluation algorithm using the raw IR images acquired using the CLT system under moving conditions. Since the CLT system continuously moves along the target structure, the FOV of the IR camera is also continuously altered in the time and spatial domains. Therefore, the IR images need to be processed for crack evaluation as following three steps.

### Step1. Time-spatial-integrated coordinate transformation

The raw IR images with the time- and spatial-varying FOV are transformed to the spatially integrated ROI images as a function of time, which is defined as the  $I^{ROI}$  image, as shown in Figure 2. The  $I^{ROI}$  image is constructed using the following time-spatial-integrated coordinate transformation. Assume that the CLT system spatially moves along only the  $x$  direction in Figure 2.

$$\begin{bmatrix} x^* \\ y \\ t^* \end{bmatrix} = \begin{bmatrix} 0 & 0 & 1 \\ 0 & 1 & 0 \\ 1 & 0 & 0 \end{bmatrix} \quad (1)$$

where the  $x$ ,  $y$  and  $z$  axes are the coordinates of the raw IR images, and the  $x^*$ ,  $y$  and  $t^*$  axes correspond to the  $I^{ROI}$  images. The  $I^{ROI}$  images can display the time-varying thermal responses in spatially fixed ROI. Here,  $x^*$  is the spatially integrated coordinate, and  $t^*$  is the time duration right before and after the line laser beam heating.

### Step 2. Phase mapping based on Hilbert transformation

Once the  $I^{ROI}$  images are reconstructed in the previous step, the phase mapping process is subsequently performed for crack visualization. If various size cracks exist in a single image, macro-cracks are typically overwhelmed while micro-cracks are hidden due to their amplitude difference. The phase mapping process overcomes the limitation related to the crack visibility issue, because the instantaneous phase information is physically self-normalized along each pixel.

First, all pixel values of the  $I^{ROI}$  images are transformed by Hilbert transformation along the  $t^*$  axis [4].

$$H(x^*, y, t^*) = \frac{1}{\pi} P \int_{-\infty}^{\infty} \frac{I^{ROI}(x^*, y, \tau)}{t^* - \tau} d\tau \quad (2)$$

where  $P$  stands for the Cauchy principle value of the integral.  $H(x^*, y, t^*)$  mathematically gives the complex numbers. Then, the instantaneous phase value of each pixel can be calculated as:

$$\theta(x^*, y, t^*) = \arctan \left( \frac{\text{Im}[H(x^*, y, t^*)]}{\text{Re}[H(x^*, y, t^*)]} \right) \quad (3)$$

where  $Re$  and  $Im$  represent the real and imaginary parts, respectively.

Next, the phase image is constructed by cumulating all phase values along the  $t^*$  axis.

$$\phi(x^*, y) = \sum_{t^*} \theta(x^*, y, t^*) \quad (4)$$

### Step 3. Spatial derivative

The phase image obtained in the previous step gives the crack-induced phase difference information, but still includes unwanted noise components. These noises can be removed by employing the spatial derivative along the scanning direction ( $x$ -direction) of the phase image.

$$F(x^*, y) = \frac{d\phi(x^*, y)}{dx^*} \quad (5)$$

where  $F$  denotes the pixel values of the final image.

## 4. EXPERIMENTAL VERIFICATION

### 4.1. Description of a target concrete specimen

A target concrete specimen with 103 MPa of compressive strength is prepared by mixing cement, silica sand, fly ash, super-plasticizer and water as shown in Figure 3. The mixing composition is summarized in Table 1. The specimen size is 1000 x 500 x 100 mm<sup>3</sup>.

Table 1. Mixing composition of the concrete specimen (%)

Cement (Type)	Silica sand	Fly ash	Super-plasticizer	Water
100 (III)	100	15	0.9	35

Then, artificial cracks are created in the concrete specimen by inserting 150  $\mu\text{m}$  acrylic slots as shown in Figure 3. The artificial cracks can be divided into two types, i.e. macro- ( $\geq 500 \mu\text{m}$ ) and micro- ( $< 500 \mu\text{m}$ ) cracks depending on their width. In addition, a fake crack is introduced by using a pencil for the positive false alarm test.

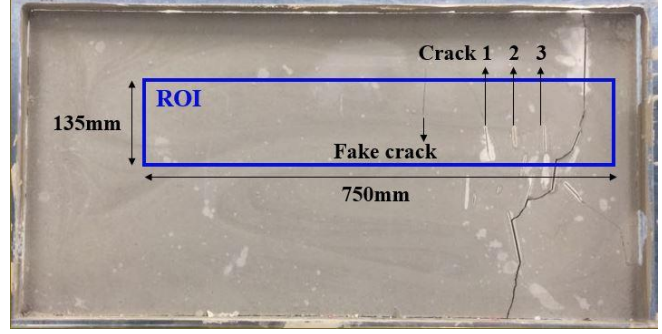


Figure 3. Target concrete specimen with various cracks

### 4. 2. Experimental setup

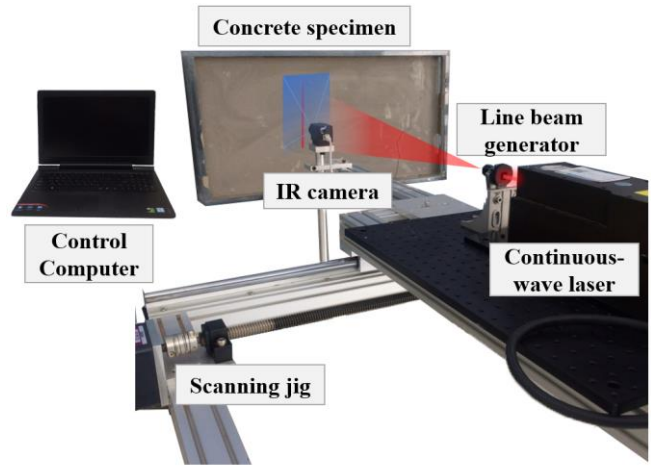


Figure 4. Experimental setup of the CLT system with a scanning jig

Figure 4 shows the experimental setup of the CLT system for concrete crack evaluation under moving condition. Here, a specially designed scanning jig is used for the moving condition of the CLT system. The continuous-wave laser (TMA-532-15T, TMA) generates a point laser beam with a wavelength of 532 nm. The point laser beam is transformed into 250 mm-long line laser beam using the line beam generator. The intensity of the line laser beam is set to approximately 111 mW/mm<sup>2</sup>. The intensity of the line laser beam is optimized by considering the scanning speed of 23 mm/s and the thermal conductivity of concrete (0.8 W/m K). The continuous-wave laser is 1600 mm apart from the concrete specimen. Then, the IR camera (A65, FLIR) measures the corresponding thermal waves in the time domain with a frame rate of 30 Hz, a spectral range of 3  $\mu\text{m}$  to 5  $\mu\text{m}$ , a pixel resolution of 640 x 512. The IR camera is 700mm away from the concrete specimen, and the corresponding FOV has height, width and spatial resolution of 135 mm, 750 mm, and 450  $\mu\text{m}$ , respectively. The scanning jig horizontally moves along ROI including fake, micro- and macro-cracks.

### 4. 3. Experimental Results

Once the raw IR images are obtained by scanning the CLT system, the  $I^{ROI}$  images can be constructed using the time-spatial-integrated coordinate transformation defined in Equation (1). Then, the phase image is obtained using Equations (2) and (3) as shown in Figure 5. However, the phase image still has a lot of noise components caused by the surface irregularity and irregular surface heating. Next, the final image of Figure 6 shows that both macro- and micro-cracks are well visualized regardless of the crack visibility issue described in Chapter 3. In Figure 7, the crack visualization results are compared with vision image captured by a HD camera. In particular, 1 mm-width macro-crack and 150  $\mu\text{m}$ -width micro-crack are successfully evaluated within 3 % error ratio as shown in Figure 7 (a). Similarly, the almost closed-type cracks having widths from 1  $\mu\text{m}$  to 50  $\mu\text{m}$  are also well detected in Figures 7 (b) and (c). On the other hand, one interesting aspect to see in Figure 7 (d) is that the fake crack is not highlighted, meaning that there is no positive false alarm. Thus, it can be inferred that the proposed technique can be used for compensating the positive false alarm of the vision image.

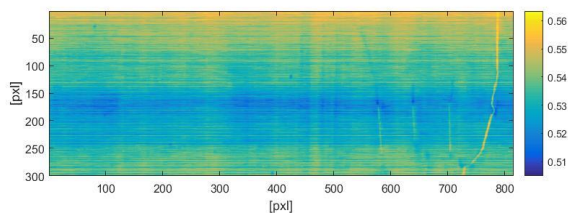


Figure 5. Phase image

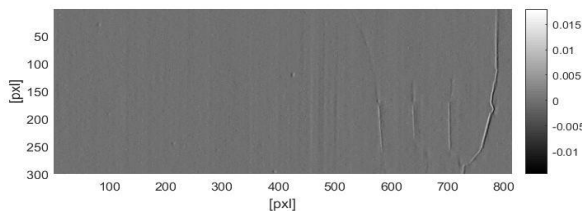


Figure 6. Final image

### 5. CONCLUSION

The continuous-wave laser thermography system and the corresponding instantaneous concrete crack evaluation algorithm are developed and experimentally validated using a lab-scale concrete specimen. The experimental results reveal that macro- and micro-cracks successfully visualized and quantified within 3% error ratio without any positive false alarms. The proposed technique can be useful as an alternative to the existing concrete crack inspection techniques. Moreover, it can be embedded onto an unmanned vehicle, making it possible to automatically inspect large scale concrete structure. Further feasibility studies for real-world applications will be followed.

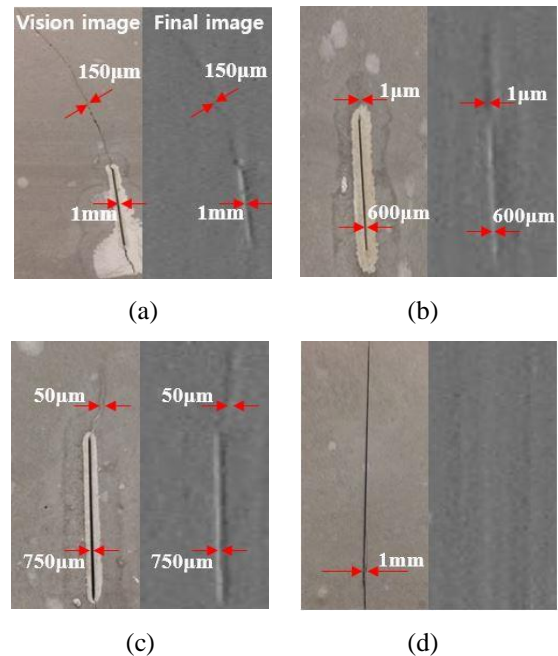


Figure 7. Comparison between vision and final images: (a) Crack 1, (b) Crack 2, (c) Crack 3 and (d) Fake crack

### References

- [1] Xuhang Tong, Jie Guo, Yun Ling, and Zhouping Yin, 'A new image-based method for concrete bridge bottom crack detection', Image Analysis and Signal Processing (IASP), 2011 International Conference on, 2011.
- [2] A.A Shah and Y Ribakov, 'Non-linear ultrasonic evaluation of damaged concrete based on higher order harmonic generation', Materials & Design, Vol 30, pp 4095-4102, 2009.
- [3] F C sham, Nelson Chen and Liu Long. 'Surface crack detection by flash thermography on concrete surface', Insight Vol50 No5 pp240-243, 2008.
- [4] Frank R. Kschischang, 'The Hilbert Transform' The Edward S. Rogers Sr. Department of Electrical and Computer Engineering University of Toronto, 2006